Landscape signature of seismogenic faults in the off- and onshore domains of the Noto Peninsula in Japan's back-arc

Luca C. Malatesta[1], Shigeru Sueoka[2], Nina-Marie Weiß[1], Boris Gailleton[3], Sumiko Tsukamoto[4,5], Daisuke Ishimura[6,7], Naoya Takahashi[8], Takuya Nishimura[9], Kyoko Kataoka[10], Tetsuya Komatsu[2], Yoshiya Iwasa[11,12]

[1]Earth Surface Process Modelling, GFZ Helmholtz Centre for Geosciences, Telegrafenberg, 14473 Potsdam, Germany
[2]Tono Geoscience Center, Japan Atomic Energy Agency, 509-5102 Toki, Japan
[3]Geosciences Rennes, University of Rennes, 35042 Rennes, France
[4]LIAG Institute for Applied Geophysics, Stilleweg 2, 30655 Hannover , Germany
[5]Department of Geosciences, University of Tübingen, Schnarrenbergstr. 94-96, 72076 Tübingen, Germany
[6]Department of Geography, Tokyo Metropolitan University, 192-0364 Hachioji, Japan
[7]Department of Earth Sciences, Chiba University, 263-8522 Chiba, Japan
[8]Department of Earth Sciences, Tohoku University, 980-8578 Sendai, Japan
[9]Disaster Prevention Research Institute, Kyoto University, 611-0011 Kyoto, Japan
[10]Research Institute for Natural Hazards and Disaster Recovery, Niigata University, 950-2181 Niigata, Japan
[11]Center for Education and Research of Disaster Risk Reduction and Redesign, Oita University, 870-1192 Oita, Japan
[12]Faculty of Education, University of Teacher Education, 811-4192 Fukuoka, Japan

Key Points:

- The faults responsible for the 2024 M_W 7.5 Noto Peninsula Earthquake likely started their activity between 326 and 238 ka.
- The nearshore bathymetry of fault-bound coasts records tectonic activity faster than the adjustment timescale of emerged landscape.
- Active faults defining the edge of uplifting land are likely found offshore but close to the coast, drowned by the current sea-level high stand.

Corresponding author: Luca C. Malatesta, `luca.malatesta@gfz.de`

Abstract

The eastern margin of the Sea of Japan is a zone of great seismic and tsunami hazard due to multiple offshore and nearshore reverse faults as shown by the 2024 M_W 7.5 Noto Peninsula Earthquake. Here we compare coseismic deformation of the 2024 Noto Peninsula Earthquake with 4767 individual marine terraces attributed to 16 successive sea-level stages over the last Myr. This reveals that the earthquake faults started slipping between 326 and 238 ka. The emerged landscape is still adjusting to it while nearshore underwater scarps mark the active faults. Applied to nearby Sado Island, these observations reveal the likely location of an active fault that drives its fast deformation. Active faults defining the edge of uplifting land are likely found in the near shore domain, drowned by the current sea-level high stand.

Plain Language Summary

Earthquakes are a major source of risk for society, through the shaking, landslides, and tsunami they can generate. Along the northwest coast of Japan, it is difficult to identify which of the multiple of active tectonic faults, are more likely to cause violent earthquakes. On January First 2024, the M_W 7.5 Noto Peninsula earthquake ruptured along one of these faults, lifting land more than four meters at the coast. This event allows us to understand the relationship between its ground deformation and the landscape of the peninsula. We find that the repetition of a similar earthquakes every 2000 years for about 250'000 years can explain many features of the peninsula. The earthquake faults are associated with an underwater scarp, a steeper slope, following the coast. On the nearby island of Sado's northwestern coast, the landscape shares many similarities with the Noto Peninsula. However, no large earthquakes have been documented along this coast over the last centuries. We find a similar underwater scarp on Sado and propose that this could be the location of a fault capable of large earthquakes.

1 Introduction

Tectonics and associated earthquakes shape landscapes. Along Japan's back-arc, seismic hazards are characterized by earthquakes up to M7 and M8 distributed on a large number of mostly offshore reverse faults (Earthquake Research Committee, 2024) uplifting inverted basins along the coast (Fig. 1) (Okamura et al., 1995). Through their shallow depths and close proximity to the coast, these faults produce strong surface shaking and short tsunami arrival times (Study Group on Research into Large-Scale Earthquakes in the Sea of Japan, 2016; Earthquake Research Committee, 2024). The rarity of earthquakes on individual faults (Earthquake Research Committee, 2024) makes it hard to identify which of the many faults are most active.

On land, surface morphology is a good proxy for the degree of fault activity because efficient subaerial erosion progressively removes inactive fault scarps (Avouac & Peltzer, 1993). This selective removal largely vanishes at water depths untouched by wave erosion where rates of erosion are extremely low (Hughes et al., 2024). The nearshore domain is in an intermediate situation, eustatic cycles periodically expose the seafloor to wave and subaerial erosion in a gradient spanning ca. -125 m to modern sea level (Jara-Muñoz et al., 2017; Johnson et al., 2017; Malatesta et al., 2021, 2022; Kluesner et al., 2023). While well-understood topographic breaks mark active faults onland (Avouac & Peltzer, 1993; Wobus et al., 2006; Picotti et al., 2009), the landscape expression of seismogenic activity is not equally well understood offshore. Here, we analyzed long-term strain from the record of 16 sea-level stages captured by over 5000 marine terraces on the Noto Peninsula and Sado Island, coseismic deformation of the 2024 M_W 7.5 Noto Peninsula earthquake, and landscape evolution modeling to gain a better understanding of the earthquake cycle topography on- and offshore in the back-arc region.
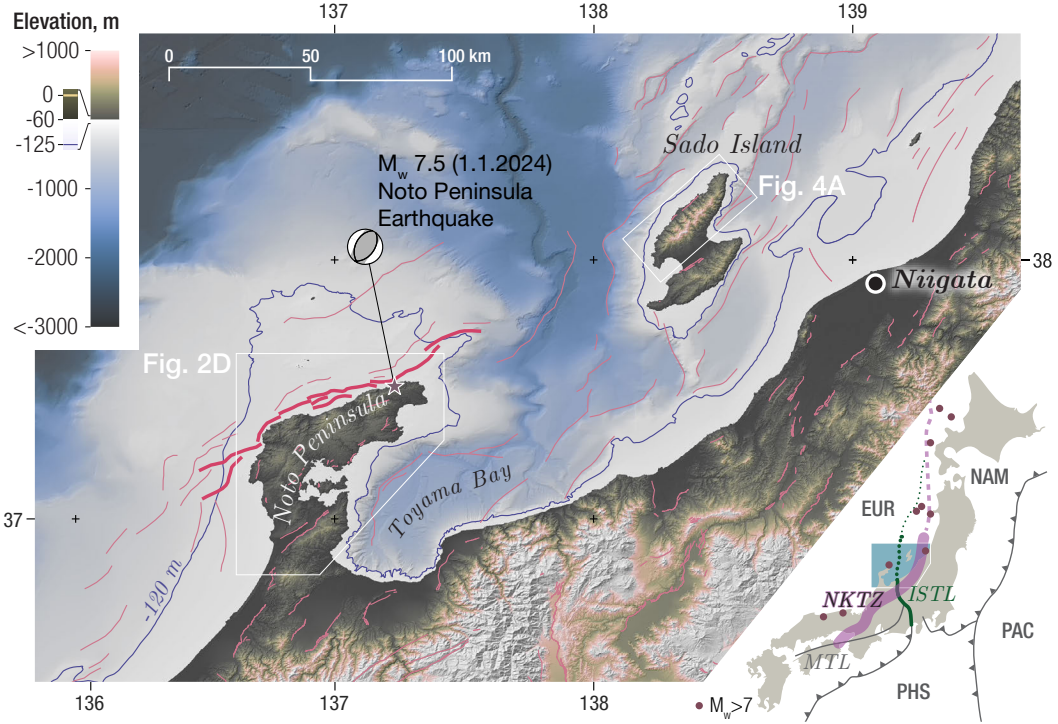
Figure 1. Regional map and tectonic context of the central coast of the Japan Sea. Mapped active faults are marked in pink, thicker ones slipped in the Noto Peninsula Earthquake (Okamura, 2019; Earthquake Research Committee, 2024). The local -120 m last sea-level low stand is traced (Gowan et al., 2025). Inset shows the main tectonic plates Eurasia (EUR), North America (NAM), Pacific (PAC), Philippine Sea (PHS); the Niigata-Kobe-Tectonic-Zone (NKTZ) (Sagiya et al., 2000), Itoigawa-Shizuoka-Tectonic-Line (ISTL), and Median-Tectonic-Line (MTL); Purple dots in inset are $M_{\mathrm{W}} > 7$ earthquakes along the Japan Sea coast since 1900. Bathymetry from Japan Hydrographic Association, topography from ASTER (ASTER Science Team, 2019).

2 Regional tectonics and earthquakes

The Noto Peninsula is marked by northeast-striking reverse faults inherited from the back-arc opening (Ishiyama et al., 2017). The area experienced extensional tectonics from ca. 25 to 13 Ma, neutral stress from ca. 13 to 3.5 Ma, and compressional deformation from ca. 3.5 Ma to the present (Sato, 1994). Reverse slip on the normal faults uplifted asymmetric inverted basins (Okamura et al., 1995). Most active reverse faults in Noto are located just offshore of its northern coastline (Fig. 1, Inoue & Okamura, 2010). Another fault system, dipping northwest, flanks the peninsula to the south on the bottom of Toyama Bay at ca. 1 km depth (Ishiyama et al., 2017). These structures occur within the Eurasia-North America diffuse plate boundary, a distributed zone that includes several fault systems. It runs along the back-arc of the Japan subduction, either offshore or along the coast according to different models (Fig. 1 inset, Nakamura, 1983; Sagiya et al., 2000; Ohzono et al., 2011; T. Tamura et al., 2020).

On 1.1.2024, a M_{W} 7.5 earthquake shook the northern coast of the Noto Peninsula (Fig. 1, 2 A–D, Ma et al., 2024; Okuwaki et al., 2024; Yoshida et al., 2024; Fukushima et al., 2024). The quake ruptured multiple southeast-dipping reverse faults off the coast and capped a 36-month period of sustained swarm activity linked to migrating fluids (Fig. S1, Nishimura et al., 2023; Yoshida et al., 2023; Kato, 2024; Japan Coast Guard & Hokuriku

Electric Power Company, 2024). As of January 2025, the earthquake cost the lives of 515 persons and close to 150,000 structures were destroyed or damaged (Cabinet Office of Disaster Management in Japan, 2025). Several faults had failed individually ($M_W > 6$) over the last decades (Inoue et al., 2007; Ozawa et al., 2008; Awata et al., 2008; Hamada et al., 2016) but a combined rupture had not been observed in historical records. Three levels of Holocene marine terraces up to 7 m high along the northwest coast of the peninsula suggest the recurrence of earthquakes with meter-scale throw at the coast (Shishikura et al., 2020).

The Noto Peninsula Earthquake tilted the land along an uplift gradient with a maximum of +4.4 m at the northwest coast and decaying to the southeast (Fig. 2 D, H, Fukushima et al., 2024). Bedrock platforms up to 200 m wide were lifted out of the water (Fig. 2 A–C, Fukushima et al., 2024; Goto et al., 2026). If the emerged volcaniclastic platforms resist wave erosion, they will become new marine terraces, record the coseismic uplift, and act as passive strain markers (Otsuka, 1932; Yoshikawa, 1964; Ota & Yoshikawa, 1978).
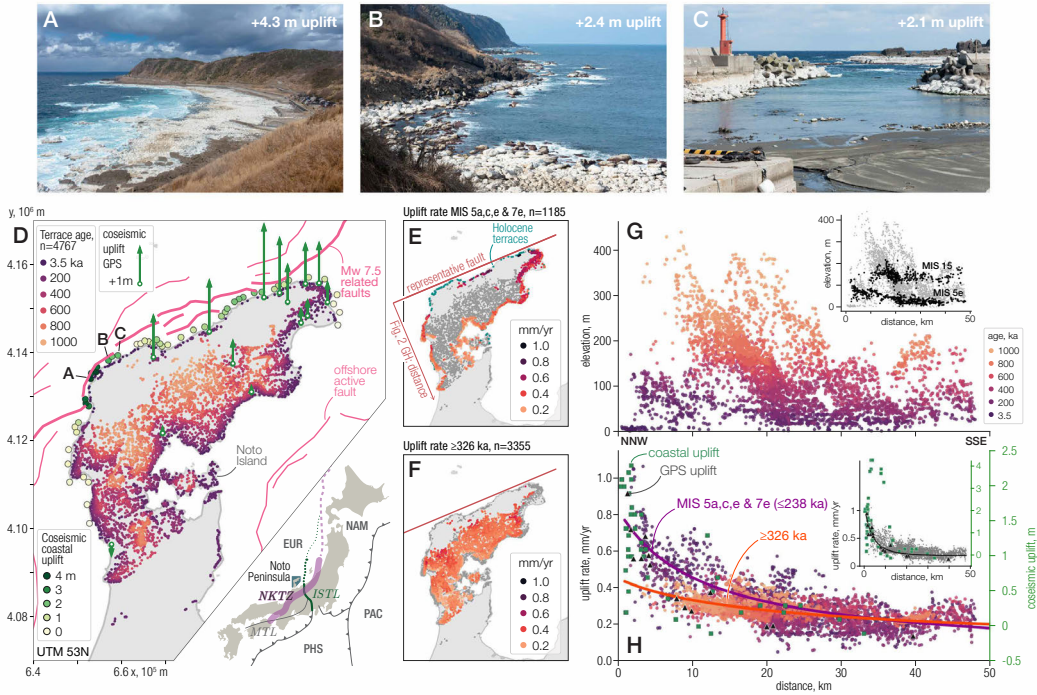

Figure 2. A–C: Coseismic uplift and coastal advance in Yoshiura, Kamiozawa, and Ozawa, March 2024. Tidal range is 0.4 m. D: Noto Peninsula with offshore active faults (Earthquake Research Committee, 2024), coseismic GPS deformation, coseismic coastal uplift (Fukushima et al., 2024), and marine terraces (Koike & Machida, 2001; Ota & Hirakawa, 1979). E: Rock uplift rate from terraces of last two interglacial highstands, MIS 5e and 7e (121 and 238 ka) and position of Holocene terraces. F: Uplift rate from terraces MIS 9e (326 ka) and older. G: Elevation and age of marine terraces along distance orthogonal to the faults' average strike (see Fig. 1 E). Inset: same data highlighting tilt of MIS 5e terraces relative to MIS 15 (572 ka). H: Uplift rates from marine terraces with power law fits for ages younger and older than 238 and 326 ka. Younger terraces show a pronounced decay similar to coseismic deformation (Nishimura et al., 2024; Fukushima et al., 2024), while older terraces, shifted by recent deformation, have a moderate decay. Inset shows the entire scale for coastal survey, and power law fit of GPS data. See Fig. S3–S5 for additional information.

3 Methods

The Noto Peninsula hosts one of the longest and best mapped series of erosive marine terraces on the globe with 4767 unique terraces (discrete mappable platforms) attributed to 16 sea-level stages over the last million years (Fig. 2 D, Ota & Hirakawa, 1979; Koike & Machida, 2001). Marine terraces result from the combined action of rock uplift and coastal erosion and can be cautiously interpreted as records of past sea-level high stands (Yoshikawa, 1964; Anderson et al., 1999; Malatesta et al., 2022). The highest terraces are correlated to Marine Isotope Stage (MIS) 29, with an age of 1.02 Ma. Radiometric age and tephro-stratigraphic constraints for MIS 5e exist in the southeast of the peninsula (Omura, 1980; Toyokura et al., 1991). Successive older terrace levels were attributed to successive sea-level high stands (Koike & Machida, 2001; Ota & Hirakawa, 1979).

We digitized the marine terraces' outline as well as those of the northern range of nearby Sado Island (537) from the *Atlas of Quaternary Marine Terraces in the Japanese Islands* (Fig. S2, Ôta, 1964; Ota & Hirakawa, 1979; Koike & Machida, 2001). We used a 1 m DEM of the Noto Peninsula provided by the Ishikawa Prefecture to trace the digitized outline of each terrace surface with improved accuracy on Noto. We recorded the elevation of the highest point of each polygon (paleo-shoreline angle, Figueiredo & Rockwell, 2022), the coordinates of their centroid and the presumed age (the entire terrace dataset and the list of shoreline markers are available as a shapefile and table in the data repository). At the time, Ota and Hirakawa (1979) used the terraces as strain markers deviating from the horizontal sea level to identify a recent phase of faster uplift in the northwest (Fig. 2 G inset). Now, we can derive the rate of rock uplift for each terrace by calculating the ratio between elevation gain from original sea level and age of the terrace and recover an uplift pattern across space and time (Fig. 2 G H). We used the sea-level reconstruction by Bintanja et al. (2005) for its 1.07 Myr length that covers all terraces of the Noto Peninsula. In the absence of radiometric controls, we relied on the published chronology assuming that successive terrace levels correspond to successive sea-level high stands (Ota & Hirakawa, 1979; Koike & Machida, 2001).

We did not derive an uplift rate from Holocene terraces. They are not radiometrically dated but proposed to span 6 to 2 ka across three levels (Shishikura et al., 2020). These ages are too close to the timescale of the earthquake cycle to capture long-term deformation. We only used a representative age of 3.5 ka for display purpose in Fig. 2 D and G. For sea-level interstages 5a and 5c, we used the revised estimates by Creveling et al. (2017) at -8.5 m and -9.4 m below present sea level respectively instead of long-term record by Bintanja et al. (2005) (-37 m and -35 m). The revised rates are coherent with terrace levels only few meters lower than MIS 5e. We excluded fast uplifting terraces on the topographic ridge to the southeast of the peninsula and the eastern part of Noto Island (Fig. 2 D) as they lie across a large active structure.

4 Results

Terraces are extensively distributed on the southeastern half of the peninsula, while only Last Interglacial (MIS 5e) and Holocene terraces are found in the northwest (Fig. 2 E, F). Coseismic uplift varies along the Noto coast and there are no MIS 5e marine terraces where it is highest (Fig. 2 D). But a MIS 5e terrace lies at ca. 85 m elevation above the mouth of the Machino River (Fig. 3) (Koike & Machida, 2001). Within 2 km along coast, coseismic uplift of the 2024 earthquake was 1.7±0.05 m (site #39, Fukushima et al., 2024). Factoring in 10% postseismic relaxation on that uplift value (Chen et al., 2024), we obtain a crude recurrence interval estimate of around 2.2 kyr for earthquakes of similar throw.

Two deformation trends emerge once terrace-derived uplift rate is plotted against
the distance from the earthquake faults (Fig. 2 G, H). Terraces of the most recent two
interglacials (MIS 5e and 7e) display a strong gradient, from up to ca. 1 mm/yr at the
highest MIS 5e terraces down to ca. 0.25±0.08 mm/yr at > 20 km from the active faults.
This trend has a similar wavelength to coseismic GPS and coastal displacement (Fig. 2 H).
But MIS 5e and 7e terraces record an additional uplift component as they still lie tens
of meter above water where coseismic uplift goes to zero. In contrast, terraces MIS 9e
(326 ka) and older all collapse around a near uniform rate of uplift of mean value 0.28±
0.06 mm/yr that still includes a tilting component from the more recent deformation.
We tested different timings for the change in deformation by back-tilting older terraces
and fitting power law decays to each group. A start of tilting between MIS 9e and 7e
yielded the lowest total error in power-law fits and MIS 11–9e is an alternative option
(supplementary text S1 and Fig. S5).

The Noto Peninsula is segmented by secondary faults that offset the elevation of
some terraces by up to tens of meters, adding scatter without obscuring dominant trends
(Ota & Hirakawa, 1979). For example, the northwestern block of the peninsula moved
independently by a few cm during the M_W 7.5 Noto Peninsula Earthquake (Fukushima
et al., 2024). Given the dominance of the tilting signal, the lack of radiometric dating
for precise strain rate estimates, and that we only aimed to identify when the main mode
of deformation shifted, we considered the peninsula as a single block and ignored mo-
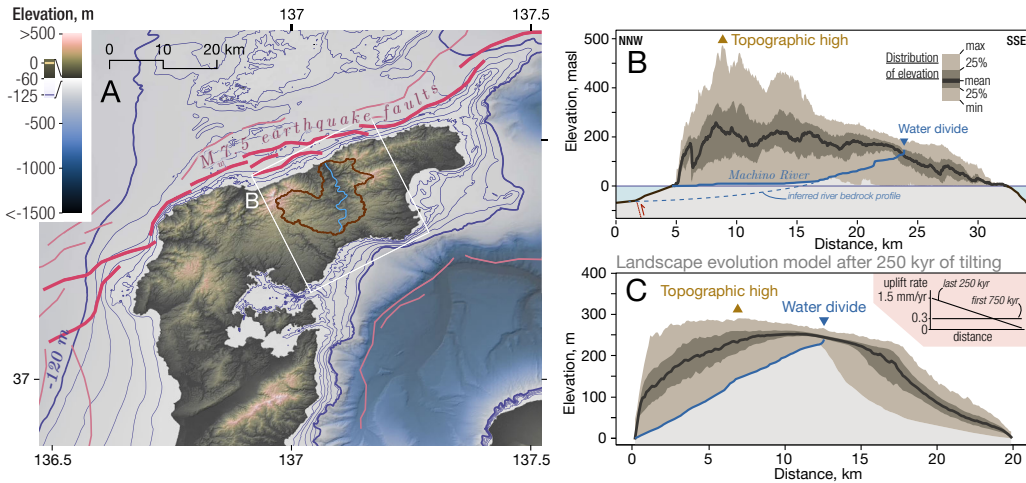tion across the sub-blocks.

Figure 3. A: Noto Peninsula with 20-m contours between sea-level low and high stand. Off-
shore active faults are traced in pink with thicker lines for the faults of the M_W 7.5 Noto Penin-
sula Earthquake (Earthquake Research Committee, 2024). The Machino River and its catchment
are traced. B: 20 km-wide topographic swath profile across the Peninsula with the projected
profile of the Machino River highlighting mismatch between drainage divide and high topog-
raphy. The footprint of the swath is shown in A. C: Swath profile across a synthetic numerical
landscape adjusting to tilting uplift. The mismatch of drainage divide and topographic high is
replicated, see Fig. S7. Bathymetry from Japan Hydrographic Association, topography from
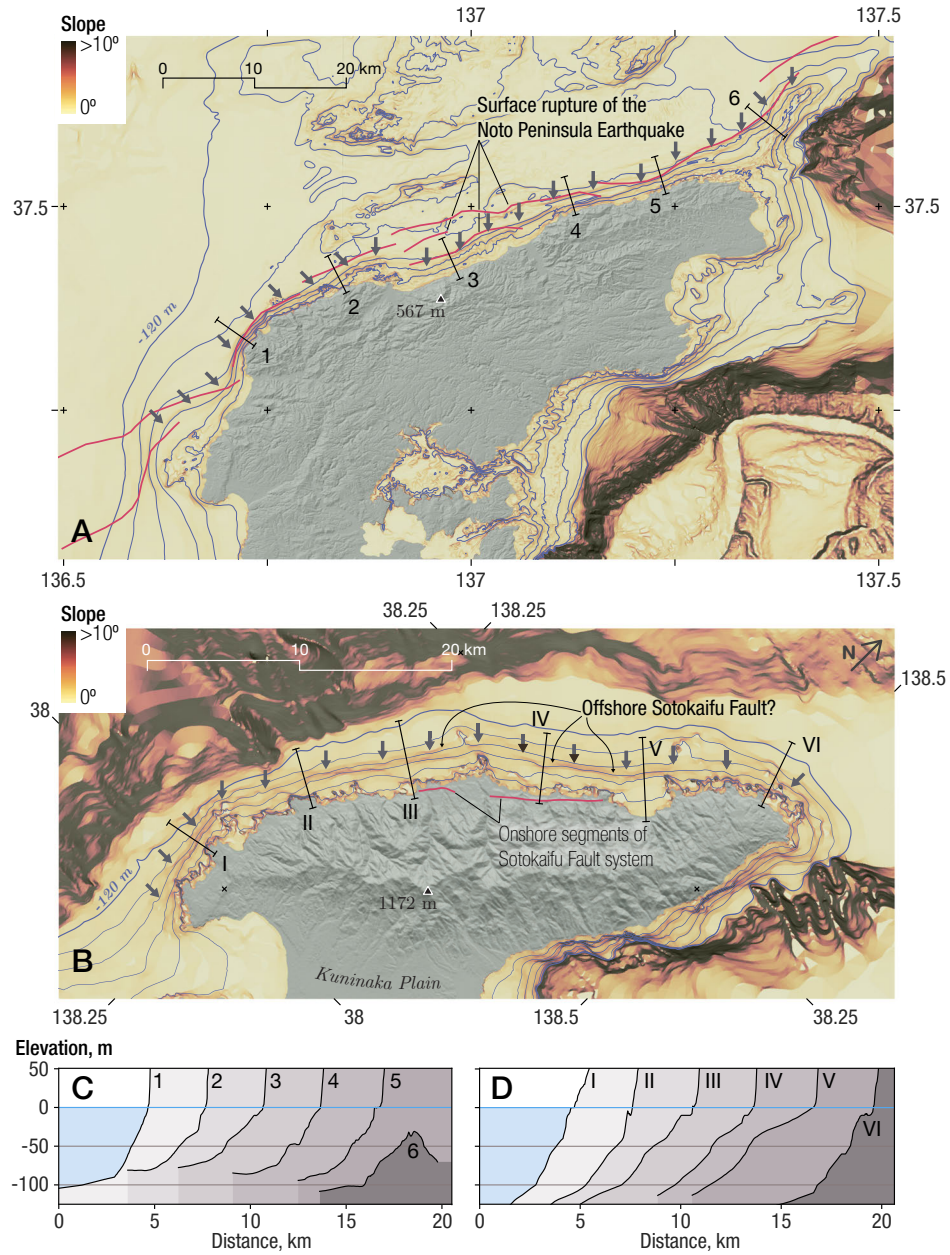ASTER (ASTER Science Team, 2019).

Figure 4. A and B: Offshore slope maps of Noto Peninsula and Oosado saturated at 10°20-m contours between sea-level low and high stand. The arrows point to the near continuous steeper scarp coinciding with the average coast. On the Noto Peninsula, this scarp matches the faults (pink lines) that ruptured during the 2024 Noto Peninsula Earthquake. Bathymetry from Japan Hydrographic Association, topography from ASTER (ASTER Science Team, 2019). C and D: profiles across the nearshore scarp on the Noto Peninsula and Sado Island with location indicated in A and B.

5 Discussion

5.1 Transient landscape response to changing tectonics

The offshore faults of the Noto Peninsula Earthquake trace a scarp at ca. -100–-50 m that marks the edge of the faster rock uplift recorded by onshore terraces (Fig. 4 A & C). The coastline follows the scarp 2–3 km landward and reflects the present short-lived sea-level high stand following a -120 m low stand during the Last Glacial Maximum (Gowan et al., 2025). The scarp is thus drowned by the current high stand and the dominant active faults are hosted in the repeatedly emerged and submerged nearshore domain.

On land, the fluvial landscape of the peninsula is not equilibrated to a faster uplift rate in the north. In the Machino River catchment, largest of the peninsula, the highest point (544 m) lies about 16 km north of the water divide (Fig. 3 B). The Machino catchment occupies nearly 90% of the width of the peninsula and reaches the sea flowing across a wide alluvial plain. At equilibrium, the uplift gradient recorded by the younger terraces would result in gentler and longer catchments draining south.

The paradox of fluvial landscape and marine terraces reflecting incompatible uplift fields can be solved considering two important points: 1) the strong tilting is a geologically recent event and the landscape currently adjusts to it, and 2) the Noto Peninsula has inherited an asymmetric topography as it emerged from the sea. The tilting of marine terraces 238 ka and younger supports the first point. The previously uniform and steady uplift rate recorded by older terraces would lead to initially steep and short catchments to the south due to the inherited submarine topography of an inverted basin (Fig. S6, Okamura et al., 1995).

We simulated the peninsula emerging from the sea with a landscape evolution model (Gailleton et al., 2024) to show how a 250 ka change from uniform to tilting uplift fields offsets highest topography and drainage divide during the transient response (Fig. 3 C, Fig. S7, supplementary text S2). The model uses stream power incision (Howard, 1994) with an implicit finite scheme described by Braun and Willett (2013) and parametrization from Ruetenik et al. (2023). The initial emerging landscape starts the strong asymmetry of an inverted basin and large catchments develop on the gentler left flank. Once the tilting uplift field starts, larger catchments can maintain a passage across the zone of faster uplift having already accumulated a large drainage area. This allows the main valleys to keep up with increased rock uplift rate, as the interfluves steepen. Rapidly, the topographic high migrates north, while the drainage divide remains south, a characteristic feature of the Noto Peninsula. Eventually, topographic high and divide converge in the north (Fig. S7).

The earlier uniform and steady uplift of Noto's inverted basin could have resulted from the north-dipping faults on the peninsula's south flank in Toyama Bay (Ishiyama et al., 2017), in potential combination with antithetic faults further north (Fig. 3 A). Marine terraces from the last million year (MIS 29–9e) document the uplift on the Peninsula's southeastern flank. The northwest flank is exposed to the stronger waves of the open sea and a beveled shelf would have widened southeastward. Between MIS 9e and 7e (326 and 238 ka), the reverse faults eventually responsible for the 2024 earthquake started slipping and led to a new and different uplift gradient across the peninsula (e.g., Ellis & Densmore, 2006; Nakajima et al., 2006). The absence of terraces older than MIS 5 on the northwest coast suggests that the coast was retreating until that time. The faults built a scarp, now offshore, that was repeatedly reworked by wave and subaerial erosion across eustatic cycles.

The initial steadiness of uplift rate derives from the assumed age model of successive terrace levels corresponding to successive sea-level high stands by Ota and Hirakawa (1979). This might not always be the case due to the morphodynamics of wave erosion

(Malatesta et al., 2022). Changes in the age or sea-level model could result in temporal variations of rock uplift rate but the nearly uniform elevation of each terrace level remains and supports the change in uplift pattern from uniform to tilting.
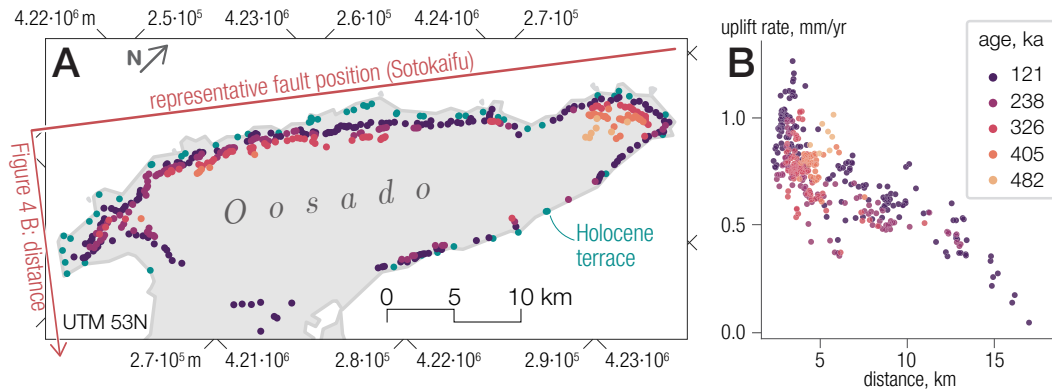

Figure 5. A: Location and age of marine terraces on Oosado (A. Tamura, 1979; Ota et al., 1992; Koike & Machida, 2001). The marker colors are shared across the subplots and indicated in B. The representative position of the Sotokaifu offshore fault is placed according to Ota et al. (1992). B: Uplift rates on Oosado as a function of distance from the proposed offshore Sotokaifu fault.

5.2 Application to the neighboring Sado Island

The relationship between landscape and seismicity exposed in the Noto Peninsula sheds light on the nearby Sado Island (Fig. 1), where data about the earthquake cycle is scant. Sado Island marks the southwestern end of the Sado Ridge (Okamura et al., 1995). Similar to the Noto Peninsula, a pattern of strong tilting to the southeast is recorded by MIS 7e and 5e terraces on Oosado, the northern range of Sado Island (Fig. 5, Fig. S8). The island is smaller, steeper, and higher (1172 m) than the Noto Peninsula and does not have an equivalent record of older terraces (Ôta, 1964). The MIS 9e–13 marine terraces are too tightly clustered at both tips of Oosado to reveal a spatial pattern of uplift (Fig. 5).

Ota et al. (1992) noted the paradox of Last Interglacial marine terraces recording a strong tilt to the southeast while the landscape of Oosado has steeper, shorter, catchments to the southeast, with evidence of stream capture and divide migration towards the northwest (Fig. 4B, Sakashita & Endo, 2023). The steeper catchments could result from past activity on the northwest-dipping reverse fault flanking the southeastern coast. That fault belongs to the series of reactivated normal faults that built the Sado Ridge since the Pliocene (Okamura et al., 1995; Watanabe et al., 1994). Ota et al. (1976, 1992) explained the recent tilting, as well as an onshore splay fault, by the activation of reverse thrusts "sometime before 300 ka" on the narrow shelf northwest of Oosado: the Sotokaifu Fault system. Due to its close proximity to the coast, the fault is not covered by existing seismic surveys and is not listed in the catalogue of "large offshore earthquake faults" (Study Group on Research into Large-Scale Earthquakes in the Sea of Japan, 2016; Okamura, 2019).

Bathymetry reveals similarities between Sado and Noto (Fig. 4). A scarp at a depth of ca. -80 to -50 m follows the Oosado coastline at a distance of 2–4 km (Fig. 4 B). At both sites, the scarp sets the upper limit of a gentle shelf and the transition to the emerged land. Its location is compatible with the offshore main segment of the Sotokaifu Fault

system proposed by Ota et al. (1992). Over 45 km long, the segment has a potential for $M \geq 7$ ruptures (Wells & Coppersmith, 1994). Based on the Noto Peninsula observations, we propose that the nearshore scarp records the position of the dominant fault system while the subaerial landscape is still adjusting to the new uplift pattern.

On Sado Island, the coseismic deformation resulting from a rupture similar to the Noto Peninsula Earthquake would cause significant uplift along the northwest coast. Most of the population, agriculture and infrastructure of the island is located in the Kuninaka Plain, southeast of Oosado. A total 24 likely tsunami deposits over the last 9 kyr identified in the plain's lacustrine system confirm that risk (Urabe, 2017). A deposit (*KAM-Ev3*) dated at 1678–1781 CE is compatible with the 1762 CE M7 Horeki Earthquake (Kawauchi, 2000). Villages in North Oosado were damaged by the tsunami of this event and its roughly estimated epicenter (Kawauchi, 2000) could match the Sotokaifu Fault system. Oosado is prone to landslides across critical roads (Shimizu & Oyagi, 1988) and the island experienced liquefaction from the distant 2024 Noto Peninsula Earthquake (Cabinet Office of Disaster Management in Japan, 2025). The similarities in recent deformation and bathymetry with the Noto Peninsula and the faster uplift rates on Sado Island warrant attention to the seismic risks from the Sotokaifu Fault.

The sole presence of a scarp at depths between 0 and -120 m in the nearshore domain is however not sufficient to derive an active tectonic interpretation. Shorter ramps also follow segments of the coast south of the Noto Peninsula and southeast of Oosado (Fig. 4). The onshore record of uplift pattern is necessary to attribute a tectonic origin to the nearshore scarp and help rank fault activity. Only the joint interpretation of onshore and nearshore topography can shed light on the nearshore bathymetry in such cases, ideally confirmed by nearshore seismic profiles (Johnson et al., 2017; Earthquake Research Committee, 2024).

6 Conclusion

The M_{W} 7.5 Noto Peninsula Earthquake of January First, 2024, provides unique information about the relationship between transient coastal landscapes and seismogenic faults characterized by long, often quiet, recurrence intervals. Repeated slip on the same fault system is responsible for the tectonic tilt on the peninsula since 324–238 ka following a previously uniform uplift. The ruptured faults are located offshore at -50 to -100 m, drowned by the current sea-level high stand. The coastline follows the continuous scarp that matches most of the faults, offset by 2–3 km. These observations can inform other sites where seismic information is limited. Nearby, the northern range of Sado Island, Oosado, shares the same pattern of recent tilting and transient landscape. Based on the Noto Peninsula, we propose that the offshore fault responsible for the tilting of Oosado is marked by a diagnostic nearshore scarp. Given the on- and offshore similarities with the Noto Peninsula, we advise increased scrutiny of seismic hazards on Sado Island.

Open Research Section

Conflict-of-interest Section

The authors have no conflicts of interest to disclose.

305 **Acknowledgments**

References

Anderson, R. S., Densmore, A. L., & Ellis, M. A. (1999, March). The generation and degradation of marine terraces. *Basin Research*, *11*(1), 7–19. doi: 10.1046/j .1365-2117.1999.00085.x

ASTER Science Team. (2019). *ASTER Global Digital Elevation Model V003.* NASA EOSDIS Land Processes Distributed Active Archive Center. doi: 10.5067/ASTER/ASTGTM.003

Avouac, J.-P., & Peltzer, G. (1993). Active Tectonics in Southern-Xinjiang, China - Analysis of Terrace Riser and Normal-Fault Scarp Degradation Along the Hotan-Qira Fault System. *Journal of Geophysical Research*, *98*, 21773–21807.

Awata, Y., Toda, S., Kaneda, H., Azuma, T., Horikawa, H., Shishikura, M., & Echigo, T. (2008, October). Coastal deformation associated with the 2007 Noto Hanto earthquake, central Japan, estimated from uplifted and subsided intertidal organisms. *Earth, Planets and Space*, *60*(10), 1059–1062. doi: 10.1186/BF03352869

Bintanja, R., Van De Wal, R. S., & Oerlemans, J. (2005, September). Modelled atmospheric temperatures and global sea levels over the past million years. *Nature*, *437*(7055), 125–128. doi: 10.1038/nature03975

Braun, J., & Willett, S. D. (2013, January). A very efficient O(n), implicit and parallel method to solve the stream power equation governing fluvial incision and landscape evolution. *Geomorphology*, *180–181*(C), 170–179. doi: 10.1016/j.geomorph.2012.10.008

Cabinet Office of Disaster Management in Japan. (2025, January). *On the damages caused by the 2024 Noto Peninsula Earthquake (in Japanese)* (Tech. Rep.). Cabinet Office of Disaster Management in Japan.

Chen, Y., Li, J., Lu, K., & Hu, T. (2024, December). Coseismic slip model and early post-seismic deformation processes of the 2024 M7.5 Noto Peninsula, Japan earthquake revealed by InSAR and GPS observations. *Geophysical Journal International*, *240*(2), 1048–1063. doi: 10.1093/gji/ggae429

Creveling, J. R., Mitrovica, J. X., Clark, P. U., Waelbroeck, C., & Pico, T. (2017, May). Predicted bounds on peak global mean sea level during marine isotope stages 5a and 5c. *Quaternary Science Reviews*, *163*, 193–208. doi: 10.1016/j .quascirev.2017.03.003

Earthquake Research Committee. (2024). *Long-term evaluation of the offshore active faults on the Japan Sea side: north of Hyogo prefecture to Joetsu region of Niigata prefecture (version August 2024, in Japanese)* (Tech. Rep.). Earthquake Research Committee.

Ellis, M. A., & Densmore, A. L. (2006). First-order topography over blind thrusts. In *Tectonics, Climate, and Landscape Evolution.* Geological Society of America. doi: 10.1130/2006.2398(15)

Figueiredo, P. M., & Rockwell, T. K. (2022). Application of Coastal Landforms to Active Tectonic Studies. In *Treatise on Geomorphology* (pp. 443–476). Elsevier. doi: 10.1016/B978-0-12-818234-5.00163-2

Fukushima, Y., Ishimura, D., Takahashi, N., Iwasa, Y., Malatesta, L. C., Takahashi, T., . . . Toda, S. (2024, December). Landscape changes caused by the 2024 Noto Peninsula earthquake in Japan. *Science Advances*, *10*(49), eadp9193. doi: 10.1126/sciadv.adp9193

Gailleton, B., Malatesta, L. C., Cordonnier, G., & Braun, J. (2024, January). CHONK 1.0: Landscape evolution framework: Cellular automata meets graph theory. *Geoscientific Model Development*, *17*(1), 71–90. doi: 10.5194/gmd-17-71-2024

Goto, H., Yamanaka, T., Makita, T., Iwasa, Y., Ogura, T., Kagohara, K., . . . Nakata, T. (2026, January). Coast uplifted by nearby shore-parallel active submarine faults during the 2024 Mw 7.5 Noto Peninsula earthquake. *Geomorphology*, *493*, 110069. doi: 10.1016/j.geomorph.2025.110069

Gowan, E. J., Tomita, T., Nishioka, D., Zhang, X., Sun, Y., Shi, X., . . . Abe-Ouchi, A. (2025, February). Impact of topographic change on the East Asian monsoon in Japan and Eastern Asia during the Last Glacial Maximum. *Progress in Earth and Planetary Science*, *12*(1), 18. doi: 10.1186/s40645-024-00681-4

Hamada, M., Hiramatsu, Y., Oda, M., & Yamaguchi, H. (2016, February). Fossil tubeworms link coastal uplift of the northern Noto Peninsula to rupture of the Wajima-oki fault in AD 1729. *Tectonophysics*, *670*, 38–47. doi: 10.1016/j.tecto.2015.12.019

Howard, A. D. (1994). A detachment-limited model of drainage basin evolution. *Water Resources Research*, *30*(7), 2261–2285. doi: 10.1029/94WR00757

Hughes, A., Olive, J.-A., Malatesta, L. C., & Escartín, J. (2024, December). Characterization of bedrock mass-wasting at fault-bound abyssal hills. *Earth and Planetary Science Letters*, *648*, 119073. doi: 10.1016/j.epsl.2024.119073

Inoue, T., Murakami, F., Okamura, Y., & Ikehara, K. (2007). Offshore Active Faults in the Source Area of the 2007 Noto Hanto Earthquake (in Japanese). *Bulletin of the Earthquake Research Institute*, *82*(4), 301.

Inoue, T., & Okamura, Y. (2010). *1:200,000 Marine Geological Map around the Northern Part of Noto Peninsula.* Geological Survey of Japan, AIST.

Ishiyama, T., Sato, H., Kato, N., Koshiya, S., Abe, S., Shiraishi, K., & Matsubara, M. (2017, July). Structures and active tectonics of compressionally reactivated back-arc failed rift across the Toyama trough in the Sea of Japan, revealed by multiscale seismic profiling. *Tectonophysics*, *710–711*, 21–36. doi: 10.1016/j.tecto.2016.09.029

Japan Coast Guard, & Hokuriku Electric Power Company. (2024). *Submarine topography survey in the northern part of the Noto Peninsula related to the 2024 Noto Peninsula earthquake* (Tech. Rep. No. 408-(3)-7). Earthquake Research Committee Meeting.

Jara-Muñoz, J., Melnick, D., Zambrano, P., Rietbrock, A., González, J., Argandoña, B., & Strecker, M. R. (2017, June). Quantifying offshore fore-arc deformation and splay-fault slip using drowned Pleistocene shorelines, Arauco Bay, Chile: Quantifying Offshore Deformation. *Journal of Geophysical Research: Solid Earth*, *122*(6), 4529–4558. doi: 10.1002/2016JB013339

Johnson, S. Y., Hartwell, S. R., Sorlien, C. C., Dartnell, P., & Ritchie, A. C. (2017, December). Shelf evolution along a transpressive transform margin, Santa Barbara Channel, California. *Geosphere*, *13*(6), 2041–2077. doi: 10.1130/GES01387.1

Kato, A. (2024, January). Implications of Fault-Valve Behavior From Immediate Aftershocks Following the 2023 M_j 6.5 Earthquake Beneath the Noto Peninsula, Central Japan. *Geophysical Research Letters*, *51*(1), e2023GL106444. doi: 10.1029/2023GL106444

Kawauchi, K. (2000). Re-Examination of the Epicenter of the 1762 Horeki off Sado Earthquake (M7.0). *Rekishi Jishin*, *16*, 107–112.

Kluesner, J. W., Johnson, S. Y., Nishenko, S. P., Medri, E., Simms, A. R., Greene, H. G., . . . Conrad, J. E. (2023, December). High-resolution geophysical and geochronological analysis of a relict shoreface deposit offshore central California: Implications for slip rate along the Hosgri fault. *Geosphere*, *19*(6), 1788–1811. doi: 10.1130/GES02657.1

Koike, K., & Machida, H. (2001). *Atlas of Quaternary Marine Terraces in the Japanese Islands.* Tokyo: University of Tokyo Press.

Ma, Z., Zeng, H., Luo, H., Liu, Z., Jiang, Y., Aoki, Y., . . . Wei, S. (2024, July). Slow rupture in a fluid-rich fault zone initiated the 2024 M_w 7.5 Noto earthquake. *Science*, eado5143. doi: 10.1126/science.ado5143

Malatesta, L. C., Bruhat, L., Finnegan, N. J., & Olive, J.-A. L. (2021, January). Co-location of the Downdip End of Seismic Coupling and the Continental Shelf Break. *Journal of Geophysical Research: Solid Earth*, *126*(1). doi:

10.1029/2020JB019589

Malatesta, L. C., Finnegan, N. J., Huppert, K. L., & Carreño, E. I. (2022). The influence of rock uplift rate on the formation and preservation of individual marine terraces during multiple sea-level stands. *Geology*, *50*, 101–105. doi: 10.1130/G49245.1

Malatesta, L. C., Weiß, N.-M., & Sueoka, S. (2025, October). *Marine terrace outlines on the Noto peninsula, Japan.* Zenodo. doi: 10.5281/zenodo.17334590

Nakajima, T., Danhara, T., Iwano, H., & Chinzei, K. (2006, November). Uplift of the Ou Backbone Range in Northeast Japan at around 10 Ma and its implication for the tectonic evolution of the eastern margin of Asia. *Palaeogeography, Palaeoclimatology, Palaeoecology*, *241*(1), 28–48. doi: 10.1016/j.palaeo.2006.06.009

Nakamura, K. (1983). Possible Nascent Trench along the Eastern Japan Sea as the Convergent Boundary between Eurasian and North American Plates. *Bulletin of the Earthquake Research Institute*, *58*(3), 711–722. doi: 10.15083/0000032948

Nishimura, T., Hiramatsu, Y., & Ohta, Y. (2023, June). Episodic transient deformation revealed by the analysis of multiple GNSS networks in the Noto Peninsula, central Japan. *Scientific Reports*, *13*(1), 8381. doi: 10.1038/s41598-023-35459-z

Nishimura, T., Hiramatsu, Y., & Ohta, Y. (2024). Source models for the 2020-2024 Noto Peninsula earthquakes based on GNSS data. In *Abstracts of JpGU Meeting 2024* (p. U16-02). Chiba, Japan.

Ohzono, M., Sagiya, T., Hirahara, K., Hashimoto, M., Takeuchi, A., Hoso, Y., . . . Doke, R. (2011, March). Strain accumulation process around the Atotsugawa fault system in the Niigata-Kobe Tectonic Zone, central Japan: Strain field around the Atotsugawa fault system. *Geophysical Journal International*, *184*(3), 977–990. doi: 10.1111/j.1365-246X.2010.04876.x

Okamura, Y. (2019, March). Distribution of Active Faults in Japan Sea and Future Issues. *Zisin (Journal of the Seismological Society of Japan. 2nd ser.)*, *71*(0), 185–199. doi: 10.4294/zisin.2017-21

Okamura, Y., Watanabe, M., Morijiri, R., & Satoh, M. (1995, September). Rifting and basin inversion in the eastern margin of the Japan Sea. *Island Arc*, *4*(3), 166–181. doi: 10.1111/j.1440-1738.1995.tb00141.x

Okuwaki, R., Yagi, Y., Murakami, A., & Fukahata, Y. (2024, June). A Multiplex Rupture Sequence Under Complex Fault Network Due To Preceding Earthquake Swarms During the 2024 Mw 7.5 Noto Peninsula, Japan, Earthquake. *Geophysical Research Letters*, *51*(11), e2024GL109224. doi: 10.1029/2024GL109224

Omura, A. (1980). 713. Uranium-series age of the Hirakodo and Uji shell beds, Noto Peninsula, Central Japan. *Transactions and proceedings of the Paleontological Society of Japan*, *117*, 247–253. doi: 10.14825/prpsj1951.1980.117_247

Ôta, Y. (1964). Coastal terraces of the Sado Island, Japan. *Geographical Review of Japan*, *37*(5), 226–242. doi: 10.4157/grj.37.226

Ota, Y., & Hirakawa, K. (1979). Marine terraces and their deformation in Noto Peninsula, Japan Sea side of Central Japan. *Geographical Review of Japan*, *52*(4), 169–189. doi: 10.4157/grj.52.169

Ota, Y., Matsuda, T., & Naganuma, K. (1976). Tilted Marine Terraces of the Ogi Peninsula, Sado Island, Central Japan, Related to the Ogi Earthquake of 1802. *Zisin (Journal of the Seismological Society of Japan. 2nd ser.)*, *29*(1), 55–70. doi: 10.4294/zisin1948.29.1_55

Ota, Y., Miyawaki, A., & Shiomi, M. (1992). Active Faults on Sado Island, off Central Japan, and Their Implication on the Marine Terrace Deformation. *Journal of Geography (Chigaku Zasshi)*, *101*(3), 205–224. doi: 10.5026/jgeography.101.205

Ota, Y., & Yoshikawa, T. (1978). Regional characteristics and their geodynamic implications of late quaternary tectonic movement deduced from deformed former shorelines in japan. *Journal of Physics of the Earth*, *26*(Supplement), S379-S389. doi: 10.4294/jpe1952.26.Supplement_S379

Otsuka, Y. (1932). Post Pliocene Crustal Movement in the Outer Zone of Southwest Japan and in the Fossa Magna. *Bulletin of the Earthquake Research Institute*, *10*(3), 701–722.

Ozawa, S., Yarai, H., Tobita, M., Une, H., & Nishimura, T. (2008, February). Crustal deformation associated with the Noto Hanto Earthquake in 2007 in Japan. *Earth, Planets and Space*, *60*(2), 95–98. doi: 10.1186/BF03352767

Picotti, V., Ponza, A., & Pazzaglia, F. J. (2009). Topographic expression of active faults in the foothills of the Northern Apennines. *Tectonophysics*, *474*, 285–294. doi: 10.1016/j.tecto.2009.01.009

Ruetenik, G. A., Jansen, J. D., Val, P., & Ylä-Mella, L. (2023, September). Optimising global landscape evolution models with 10Be. *Earth Surface Dynamics*, *11*(5), 865–880. doi: 10.5194/esurf-11-865-2023

Sagiya, T., Miyazaki, S., & Tada, T. (2000). Continuous GPS Array and Present-day Crustal Deformation of Japan. *Pure appl. geophys.*, *157*.

Sakashita, A., & Endo, N. (2023, January). Mobility and Location of Drainage Divides Affected by Tilting Uplift in Sado Island, Japan. *Remote Sensing*, *15*(3), 729. doi: 10.3390/rs15030729

Sato, H. (1994, November). The relationship between Late Cenozoic tectonic events and stress field and basin development in northeast Japan. *Journal of Geophysical Research: Solid Earth*, *99*(B11), 22261–22274. doi: 10.1029/94JB00854

Shimizu, F., & Oyagi, N. (1988). *National Research Institute for Earth Science and Disaster Prevention, Landslide topography distribution map Volume 4 "Murakami and Sado"* (109th ed.). National Research Center for Disaster Prevention.

Shishikura, M., Echigo, T., & Namegaya, Y. (2020). Activity of the off-shore active faults along the northern coast of the Noto Peninsula deduced from the height distribution of the lower marine terrace and emerged sessile assemblage. *Active Fault Research*, *53*, 33–49.

Study Group on Research into Large-Scale Earthquakes in the Sea of Japan. (2016). *Report of the Study Group on Large-Scale Earthquakes in the Sea of Japan (in Japanese)* (Tech. Rep.). Ministry of Land, Infrastructure, Transport and Tourism.

Tamura, A. (1979). Holocene marine terraces and crustal movements of Sado Island, Central Japan. *Geographical Review of Japan*, *52*(7), 339–355. doi: 10.4157/grj.52.339

Tamura, T., Oohashi, K., Otsubo, M., Miyakawa, A., & Niwa, M. (2020, December). Contribution to crustal strain accumulation of minor faults: A case study across the Niigata–Kobe Tectonic Zone, Japan. *Earth, Planets and Space*, *72*(1), 7. doi: 10.1186/s40623-020-1132-5

Toyokura, I., Ohmura, K., Arai, F., Machida, H., Takase, N., Nakadaira, K., & Ito, T. (1991). Identification of the Sambe Kisuki Tephra found in Marine Terrace Deposits along Coastal Areas of Hokuriku District, and its Implications. *The Quaternary Research (Daiyonki-Kenkyu)*, *30*(2), 79–90. doi: 10.4116/jaqua.30.79

Urabe, A. (2017, October). Reconstruction of tsunami history based on event deposits in the Niigata area, eastern coast of the Sea of Japan. *Quaternary International*, *456*, 53–68. doi: 10.1016/j.quaint.2017.05.045

Watanabe, M., Okamura, Y., & Satoh, M. (1994). Diatom fossil and geologic structure of the southeastern margin (off Tohoku) of the Japan Sea. *Bulletin of Geological Survey of Japan*, *45*, 405–436.

Wells, D. L., & Coppersmith, K. J. (1994, August). New empirical relationships among magnitude, rupture length, rupture width, rupture area, and surface displacement. *Bulletin of the Seismological Society of America*, *84*(4), 974–1002. doi: 10.1785/BSSA0840040974

Wobus, C. W., Whipple, K. X., Kirby, E., Snyder, N., Johnson, J., Spyropolou, K., ... Sheehan, D. (2006). Tectonics from topography: Procedures, promise, and pitfalls. *Geological Society of America Special Paper*, *398*, 55–74. doi: 10.1130/2006.2398(04)

Yoshida, K., Takagi, R., Fukushima, Y., Ando, R., Ohta, Y., & Hiramatsu, Y. (2024, August). Role of a Hidden Fault in the Early Process of the 2024 M$_w$ 7.5 Noto Peninsula Earthquake. *Geophysical Research Letters*, *51*(16), e2024GL110993. doi: 10.1029/2024GL110993

Yoshida, K., Uchida, N., Matsumoto, Y., Orimo, M., Okada, T., Hirahara, S., ... Hino, R. (2023, November). Updip Fluid Flow in the Crust of the Northeastern Noto Peninsula, Japan, Triggered the 2023 M_w 6.2 Suzu Earthquake During Swarm Activity. *Geophysical Research Letters*, *50*(21), e2023GL106023. doi: 10.1029/2023GL106023

Yoshikawa, T. (1964). On the Geomorphic Development of Ria Coasts in the Japanese Islands. *The Quaternary Research (Daiyonki-Kenkyu)*, *3*(5), 290–296. doi: 10.4116/jaqua.3.290

Supporting Information for "Earthquake faults recorded in the near-shore bathymetry of Japan's back-arc"

Luca C. Malatesta[1], Shigeru Sueoka[2], Nina-Marie Weiß[1], Boris Gailleton[3],

Sumiko Tsukamoto[4,5], Daisuke Ishimura[6,7], Naoya Takahashi[8], Takuya

Nishimura[9], Kyoko Kataoka[10], Tetsuya Komatsu[2], Yoshiya Iwasa[11]

[1]Earth Surface Process Modelling, GFZ Helmholtz Centre for Geosciences, Telegrafenberg, 14473 Potsdam, Germany

[2]Tono Geoscience Center, Japan Atomic Energy Agency, 509-5102 Toki, Japan

[3]Geosciences Rennes, University of Rennes, 35042 Rennes, France

[4]LIAG Institute for Applied Geophysics, Stilleweg 2, 30655 Hannover , Germany

[5]Department of Geosciences, University of Tübingen, Schnarrenbergstr. 94-96, 72076 Tübingen, Germany

[6]Department of Geography, Tokyo Metropolitan University, 192-0364 Hachioji, Japan

[7]Department of Earth Sciences, Chiba University, 263-8522 Chiba, Japan

[8]Department of Earth Sciences, Tohoku University, 980-8578 Sendai, Japan

[9]Disaster Prevention Research Institute, Kyoto University, 611-0011 Kyoto, Japan

[10]Research Institute for Natural Hazards and Disaster Recovery, Niigata University, 950-2181 Niigata, Japan

[11]Center for Education and Research of Disaster Risk Reduction and Redesign, Oita University, 870-1192 Oita, Japan

October 10, 2025, 5:30pm

Contents of this file

1. Text S1 and S2

2. Figures S1 to S6

3. Table S1

Additional Supporting Information (Files uploaded separately)

1. Captions for Dataset S1

2. Captions for Dataset S2

Introduction

Text S1. Trends in uplift rates from marine terraces

To identify the time when deformation of the Noto Peninsula started to be dominated by slip on the northwest fault, we analyzed patterns of uplift rates recorded by the marine terraces. The gradient in uplift reflected by the younger terraces impacted all older terraces and we tested the effect of changing the mode of deformation at cut-offs set between each of the marine terrace levels (MIS 5 to 29). We "back-tilted" the older terraces (Fig. S5 A) by subtracting the elevation gain gradient identified in the younger terraces. To do so, we fitted an power law decay to the terraces younger than the cutoff (red line

————

Corresponding author: L. C. Malatesta, Earth Surface Process Modelling, GFZ Helmholtz Centre for Geosciences, Telegrafenberg, 14473 Potsdam, Germany. (luca.malatesta@gfz.de)

October 10, 2025, 5:30pm

in Fig. S5 B) of the form:

$$y = \frac{a}{(x+c)^b} \, ,$$

where parameters a, b, and c are strictly positive to fit a decreasing trend away from the origin. The tilting is superimposed over a background rock uplift (assumed uniform) as the coseismic deformation is null in areas far from the fault where MIS 5 terraces are nevertheless tens of meters above sea level (Fig. 2 H). We derived the amount of corrective back-tilting by removing the background rate of rock uplift from the power law and multiplied it by the age of the cutoff. Increasingly older cut-offs yield greater magnitudes of back-tilting (Fig. S5 C and D).

We then fitted the same power law to the uplift rate derived from the back-tilted terraces older than the cut-off (blue line in Fig. S5 B and D). We could then track the goodness of fit and the parameters of the power law for all potential cut-offs (Fig. S5 E). The total root mean square errors (RMSE) of the power laws on either side of the cutoff (taking the square root of the summed squared RMSE of both fits) captures the opposing trends of: 1) increasing errors when fitting a power law to the back-tilted terraces with increasing cut-offs and 2) the reduced error of a power law fitted to the younger terraces as the cut off increases (Fig. S5 F). The minimum in total error is for a switch in deformation between MIS 7 and 9.

Finally, we tracked the exponent b of the power law fitted to the uplift rate from the back-tilted terraces (Fig. S5 F). The best fit of a power law decay requires an exponent of $b = 0$ once only terraces of age MIS 11 and above are considered, i.e., the power law decay signature of the coseismic deformation is completely absent. The limits forcing the

power law to have a negative slope make it very close to a horizontal linear trend for MIS 9–11 cut-offs and older (when b is near zero, Fig. S5 F).

Text S2. Landscape evolution model

To explore the likelihood of the Noto Peninsula being a transient landscape, we employ a landscape evolution model (Gailleton et al., 2024) to simulate the emergence of an inverted basin and its later tilting (Main text Fig. 3 C, and Fig S7). The simulation does not seek to capture all processes at play, such as ocean waves, sedimentation, and second-order faults (Ota & Hirakawa, 1979). It focuses on the transient response of the fluvial system to the changing tectonics, a fundamental aspect of the landscape. We keep track of the first-order morphology to reasonably compare this simplified model with the complex reality.

We model fluvial erosion using the stream power incision (Howard, 1994) with an implicit finite scheme described by Braun and Willett (2013). The governing equation is as follow:

$$\frac{dz}{dt} = U(x) - K\,A(x)^m \left(\frac{dz}{dx}\right)^n$$

Where z is the elevation [L], x the distance along 1D flow lines following the steepest descent [L], A the drainage area [L^2] and K the erodibility [L^{-2}m+1/T], encompassing rock strength and other local processes. We use $n = 1.11$, matching observations for that drainage area (Ruetenik et al., 2023) and $m = 0.45$. We calibrated $K = 4 \cdot 10^{-5}$ to reproduce the relief and elevation range observed at the field site.

We approximate the peninsula with a 60 by 40 km domain progressively emerging from the sea (Fig. S7). The southern edge is steep to resemble the edge of the Toyama Bay,

while the rest of the domain slopes gently to the north. After 750 kyr of uniform rock uplift, a fault breaks in the upper third of the domain and tilts the southern section with 1.5 mm/yr uplift to the north for 250 kyr. The emerging landscape first inherits a strong asymmetry despite the uniform uplift. The larger north-flowing catchments can then cross the newly established zone of faster uplift having already accumulated a large drainage area. This allows the main valleys to keep up with increased rock uplift rate, while the interfluves steepen. Rapidly, the highest topography grows in the north, while the drainage divide remains in the south, a characteristic feature of Noto (Fig. **??**B). This period of offset topographic high and drainage divide lasts for ca. 300 kyr under these parameters and ends when the topographic high and the water divide get closer again as the landscape finishes adjusting to the new forcing (Fig. S7 G).

October 10, 2025, 5:30pm

Data Set S1.

ds01.csv: Age, location, and elevation of all the marine terraces from Koike and Machida (2001) used in this article.

Data Set S2.

Noto_Sado_terraces.zip: Shapefile format with outline of all terraces on the Noto Peninsula and Sado Island from Koike and Machida (2001).

References

Braun, J., & Willett, S. D. (2013, January). A very efficient O(n), implicit and parallel method to solve the stream power equation governing fluvial incision and landscape evolution. *Geomorphology*, *180–181*(C), 170–179. doi: 10.1016/j.geomorph.2012.10.008

Gailleton, B., Malatesta, L. C., Cordonnier, G., & Braun, J. (2024, January). CHONK 1.0: Landscape evolution framework: Cellular automata meets graph theory. *Geoscientific Model Development*, *17*(1), 71–90. doi: 10.5194/gmd-17-71-2024

Howard, A. D. (1994). A detachment-limited model of drainage basin evolution. *Water Resources \ldots*, *30*(7), 2261–2285. doi: 10.1029/94WR00757

Japan Coast Guard, & Hokuriku Electric Power Company. (2024). *Submarine topography survey in the northern part of the Noto Peninsula related to the 2024 Noto Peninsula earthquake* (Tech. Rep. No. 408-(3)-7). Earthquake Research Committee Meeting.

Koike, K., & Machida, H. (2001). *Atlas of Quaternary Marine Terraces in the Japanese Islands.* Tokyo: University of Tokyo Press.

Ota, Y., & Hirakawa, K. (1979). Marine terraces and their deformation in Noto Peninsula,

Japan Sea side of Central Japan. *Geographical Review of Japan*, *52*(4), 169–189. doi: 10.4157/grj.52.169

Ruetenik, G. A., Jansen, J. D., Val, P., & Ylä-Mella, L. (2023, September). Optimising global landscape evolution models with 10Be. *Earth Surface Dynamics*, *11*(5), 865–880. doi: 10.5194/esurf-11-865-2023
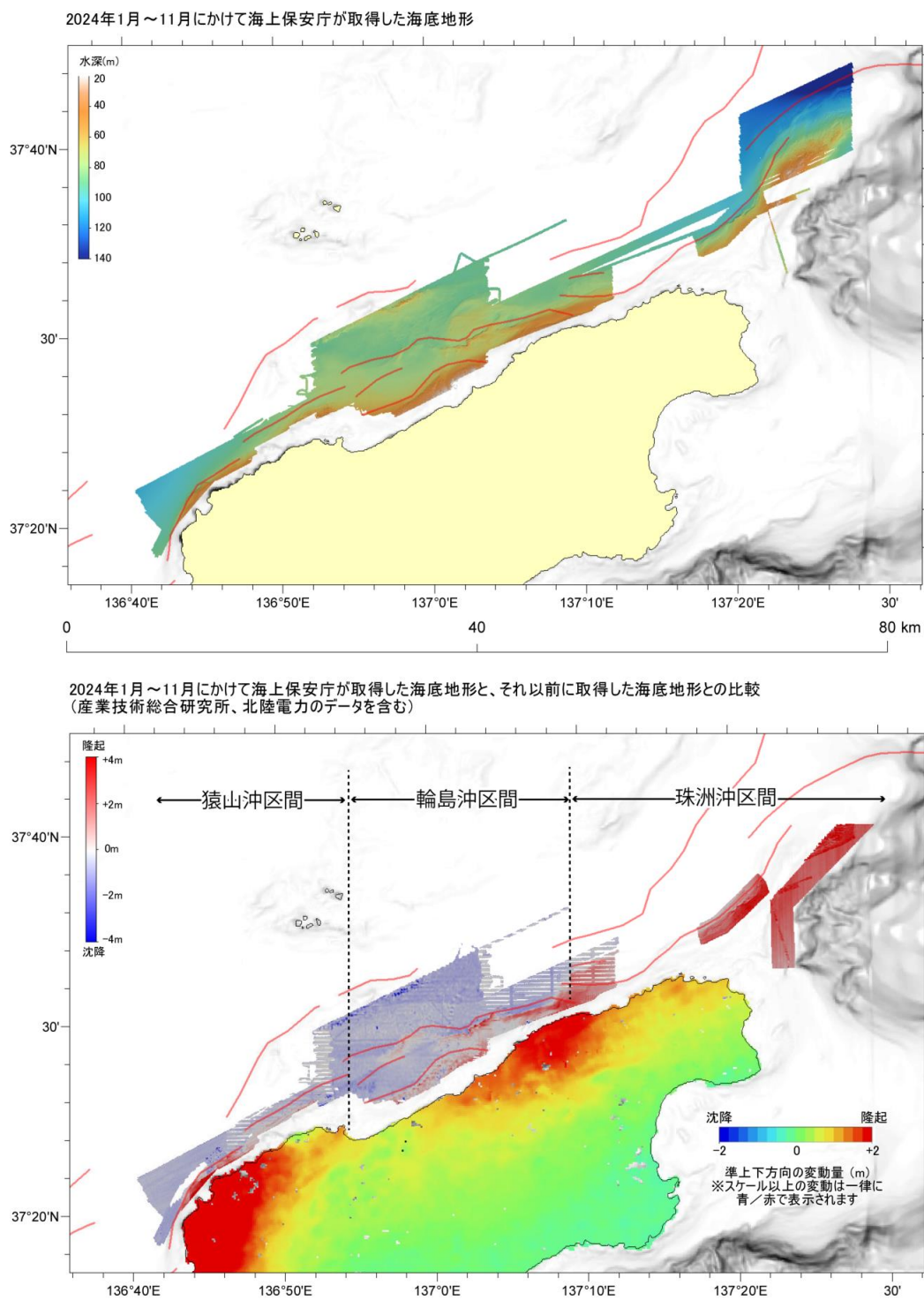
October 10, 2025, 5:30pm

Figure S1.   Reproduction of Figure 4 *"Post-earthquake seafloor topography (Japan Coast Guard) and distribution of topographical changes before and after the earthquake"* from the report by Japan Coast Guard and Hokuriku Electric Power Company (2024) in the Earthquake Research Committee Meeting 408-(3)-7.

October 10, 2025, 5:30pm
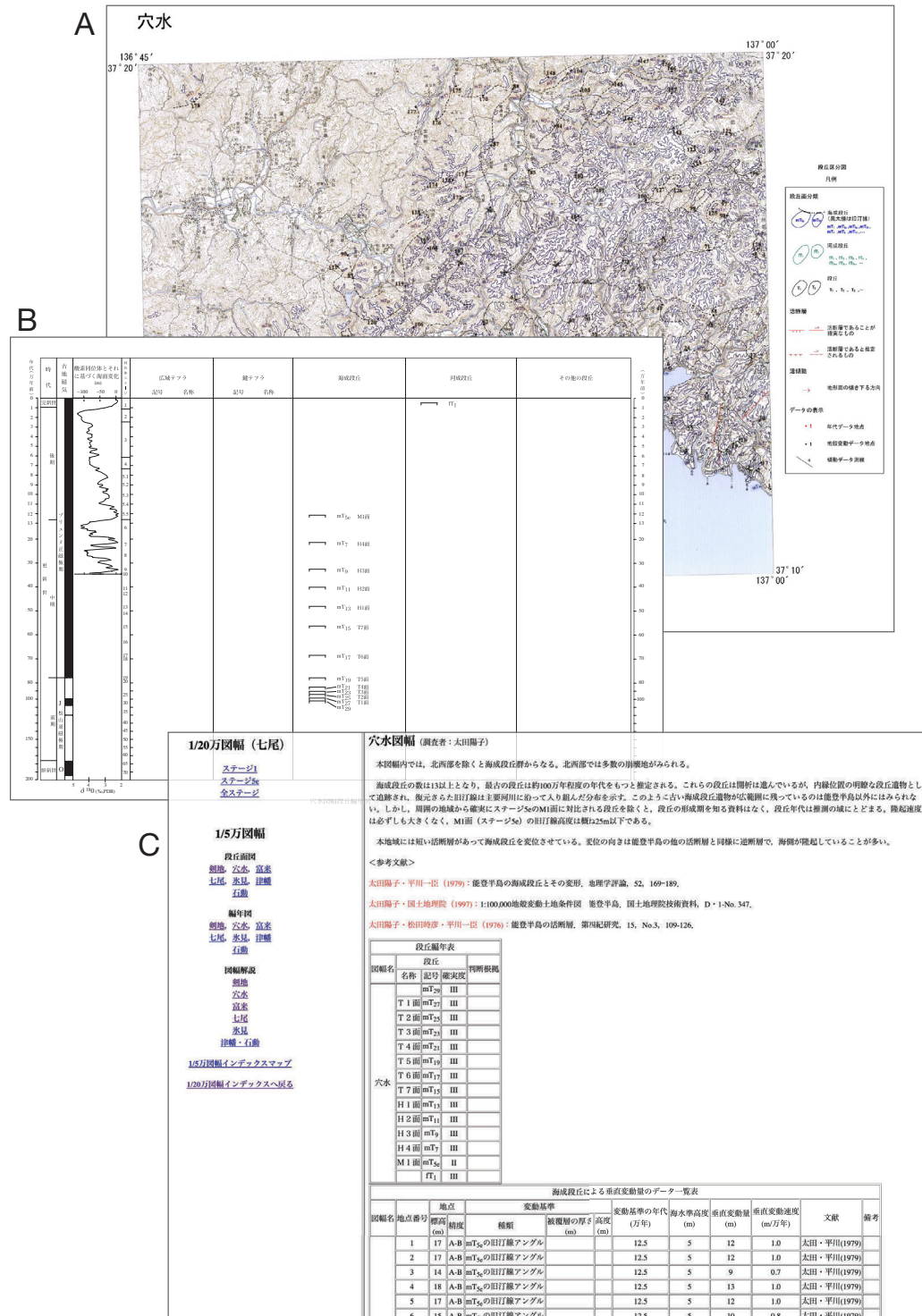
Figure S2. Screenshots from the Atlas of Quaternary Marine Terraces in the Japanese Islands by Koike and Machida (2001). A: map of the Anamizu quadrant with marine terraces outlines labeled, and the location of constraint points from the literature (numbered black dots). B: position of terrace levels in the Anamizu quadrant on a chronostratigraphic table. Summary of observations written by Yoko Ota, responsible for that quadrant, and reference for the constraint points.
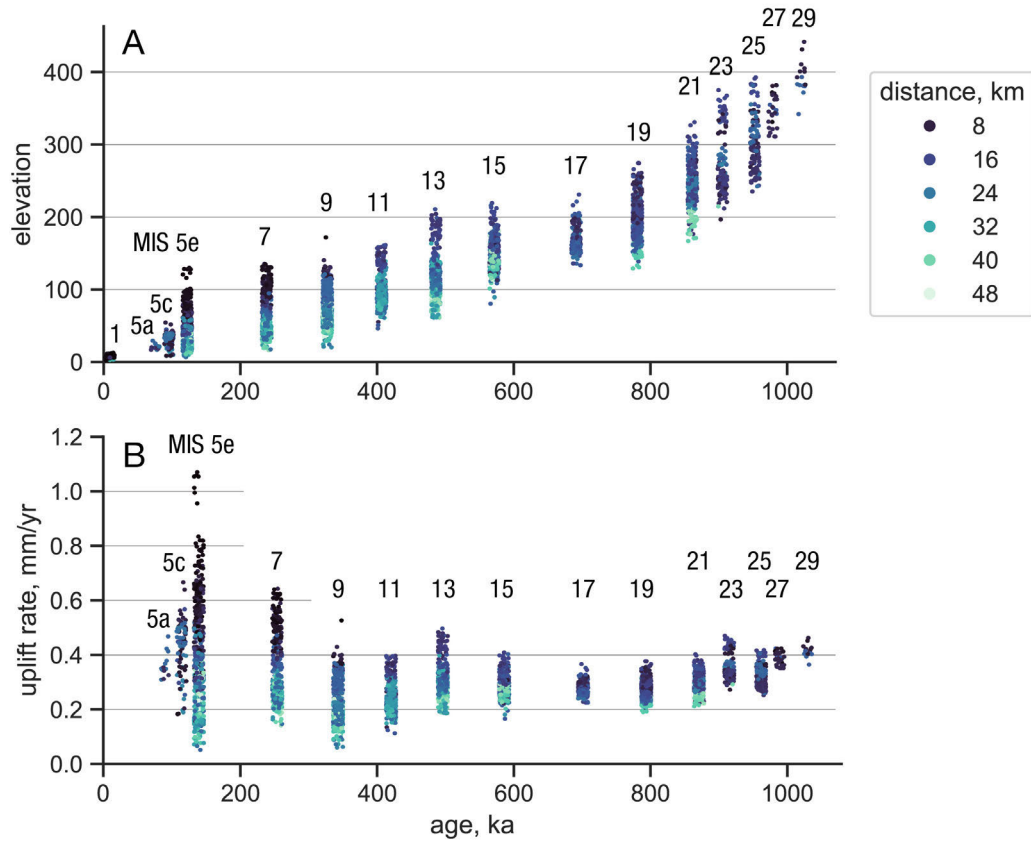
October 10, 2025, 5:30pm

Figure S3.   Same data as in Fig. 2. A: marine terrace elevation as a function of age and colored by distance from the reference fault trend. B: respective uplift rates presented in the same manner. The horizontal scatter for each age is only there for visualization purposes.
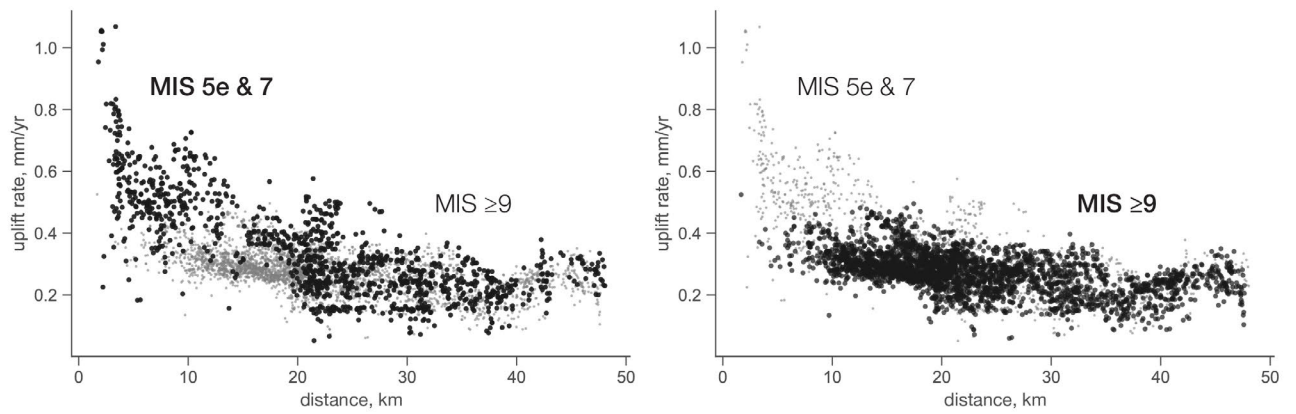
October 10, 2025, 5:30pm

Figure S4. Rate of uplift recorded by marine terraces separating the last two interglacials (MIS 5e and 7e) on the left and all terraces of age MIS 9e and older. Same data as Fig. 2 B.
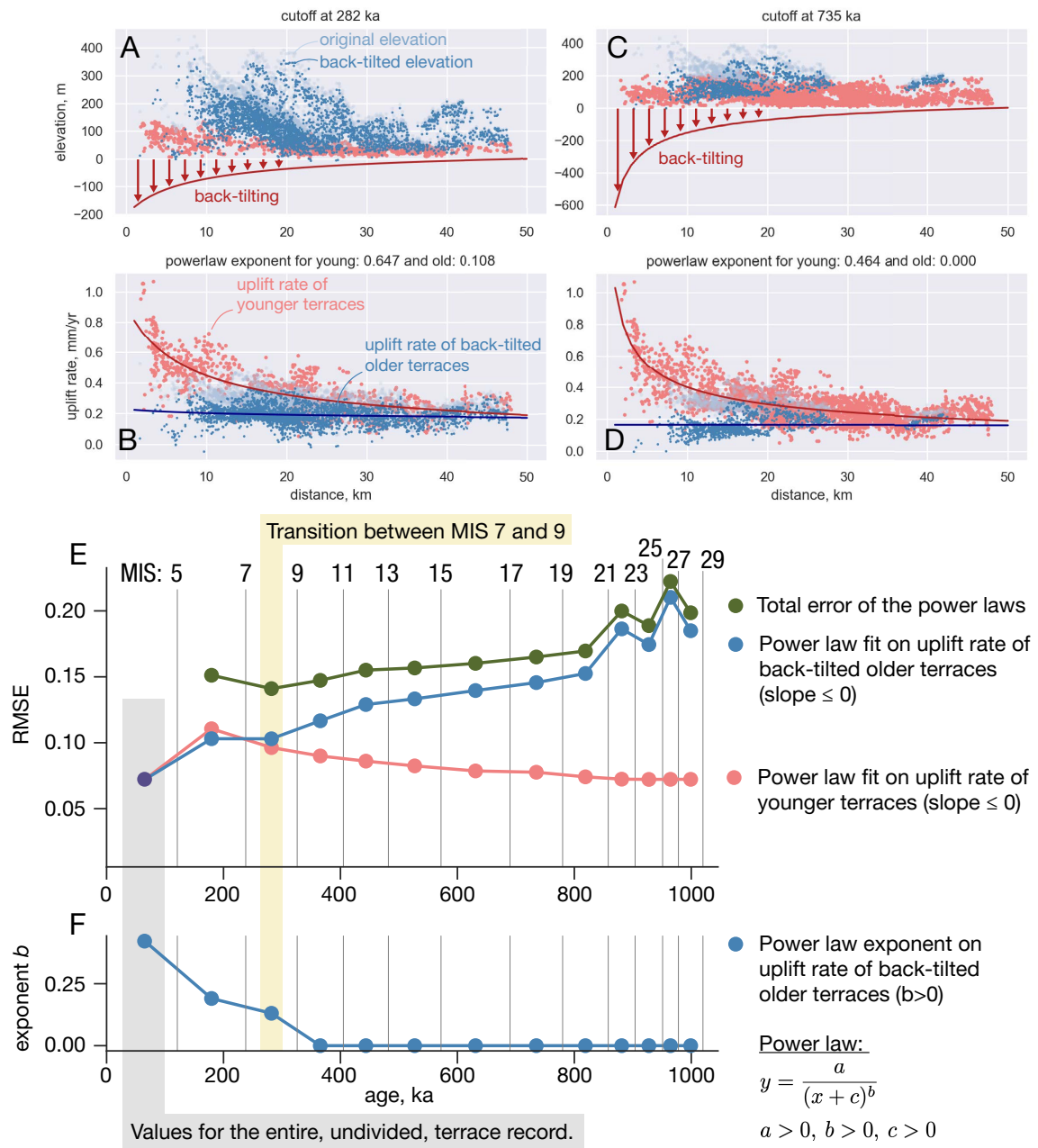
Figure S5. See text S1. A: elevation of terraces with terraces older than 282 ka back-tilted after removing a power law decay fitted on the uplift rate of the terraces younger than 282 ka (B). C & D, same as A & B but for a cut-off at 735 ka. E. Root Mean Square Errors (RMSE) for power-law fits of uplift rates from terraces younger and older than the cut-off (x-axis). F value of exponent b on the power-law fit of uplift rates for terraces older than the cut off.

Fig. 5   Seismic profile of the Torimiguri Bank showing typical basin inversion. See Fig. 4 for location.

Figure S6.   Reproduction of Figure 5 from the article by Okamura, Y., Watanabe, M., Morijiri, R., & Satoh, M. (1995): Rifting and basin inversion in the eastern margin of the Japan Sea. Island Arc, 4(3), 166–181. doi:10.1111/j.1440-1738.1995.tb00141.x .
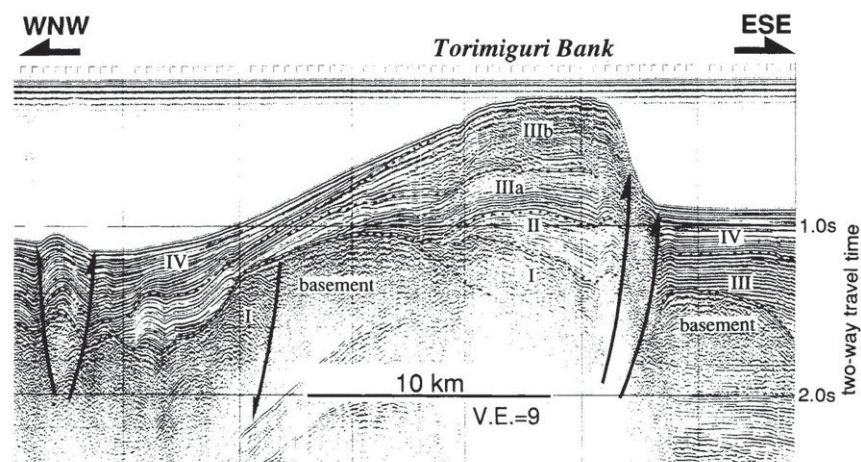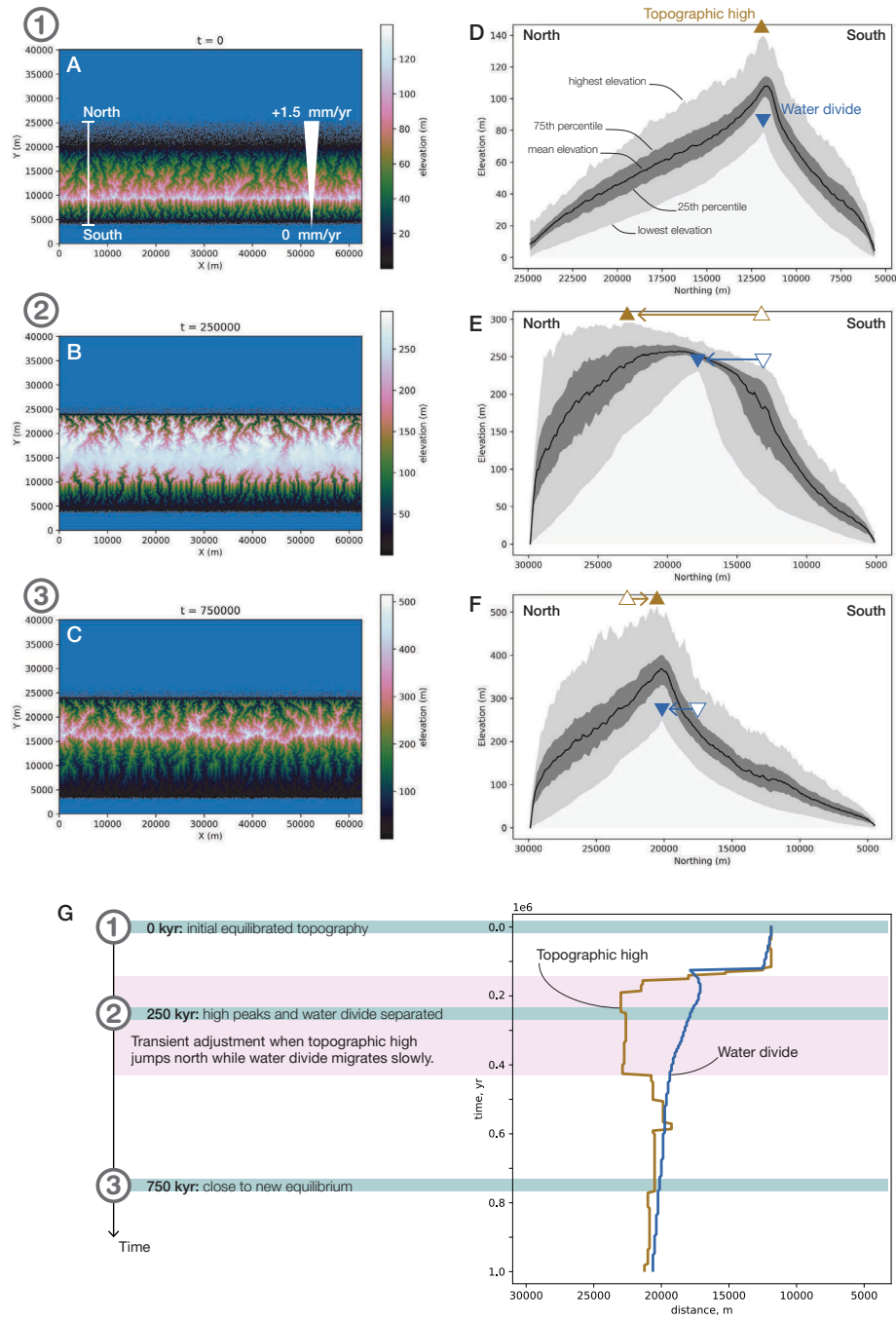
October 10, 2025, 5:30pm

Figure S7. Overview of the landscape evolution model. A to C: Map-view of the landscape responding an uplift gradient faster to the north starting at $t = 0$ from an equilibrated asymmetric ridge inherited from an inverted basin. D to F: North-south swath profiles across the range showing the minimum, maximum, 25th, 75th percentiles, and mean elevations as well as the location of the highest peak and lowest drainage divide. G: Trajectory of topographic high and water divide through time as the model run adjusts to a new uplift field.
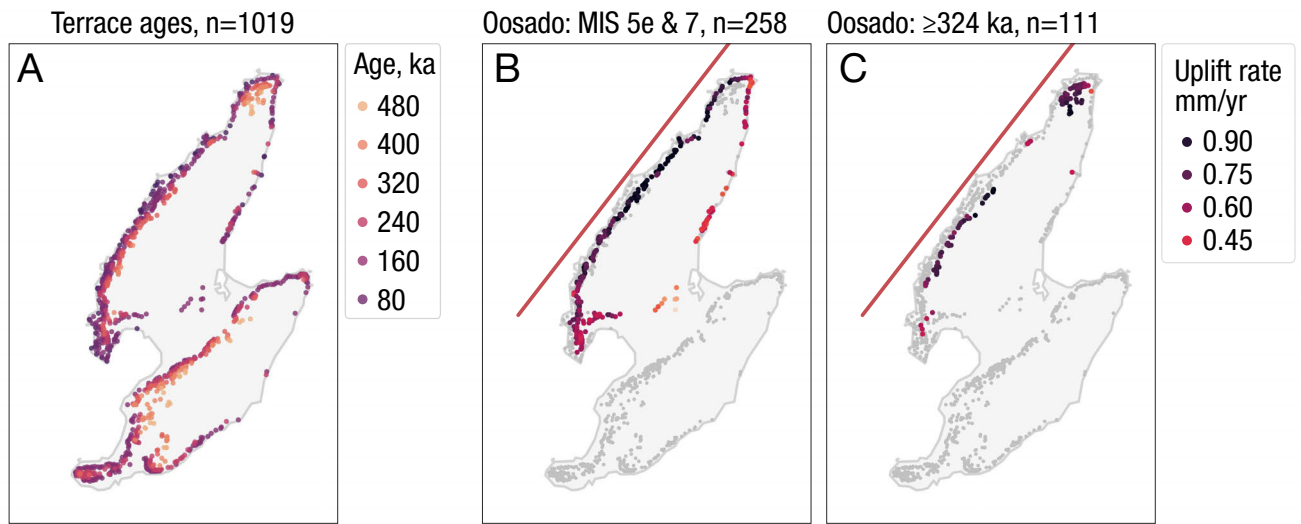
October 10, 2025, 5:30pm

Figure S8. A: age of marine terraces on Sado Island. B: uplift rates derived from the last two interglacial marine terraces in the northern range of Oosado. C: same as B for terraces older than the last two interglacials (MIS 9e, 11, and 13).

Table S1. Coseismic displacement recorded by GPS stations on the Noto Peninsula.

Station ID	Latitude (°)	Longitude (°)	EW (m)	NS (m)	UD (m)
00NTYD	137.0926	37.3659	-0.9345	0.0429	0.4867
00SZHK	137.2837	37.5258	-1.8135	1.2373	0.9677
00SZID	137.2871	37.46	-0.7186	0.0637	0.2733
00SZMS	137.3392	37.4869	-0.9202	0.1494	0.4008
00SZOT	137.1764	37.5	-1.1932	0.59	1.9024
20971	137.034	37.4323	-1.9561	-0.5349	1.2881
20972	136.9088	37.2264	-0.9142	0.2463	0.0115
71158	136.7727	37.0007	-0.0958	0.0021	-0.1374
229094	137.3188	37.5265	-1.1221	0.2164	0.9714
229095	137.2368	37.4896	-0.8895	-0.3509	0.8833
940053	136.8892	37.3824	-1.2144	-0.2188	1.017
950253	137.27	37.446	-0.7905	0.0358	0.223
960574	137.1386	37.307	-0.6628	0.2259	0.0006
00SZMT	137.2167	37.5084	-1.6584	0.7963	1.3877